

---

This is an electronic reprint of the original article.  
This reprint may differ from the original in pagination and typographic detail.

Lee, Hsin Ju; Huang, Shu Yu; Kuo, Wen Jui; Graham, Simon J.; Chu, Ying Hua; Stenroos, Matti; Lin, Fa Hsuan

**Concurrent electrophysiological and hemodynamic measurements of evoked neural oscillations in human visual cortex using sparsely interleaved fast fMRI and EEG**

*Published in:*  
NeuroImage

*DOI:*  
[10.1016/j.neuroimage.2020.116910](https://doi.org/10.1016/j.neuroimage.2020.116910)

Published: 15/08/2020

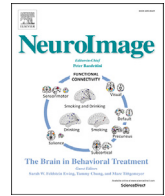
*Document Version*  
Publisher's PDF, also known as Version of record

*Published under the following license:*  
CC BY-NC-ND

*Please cite the original version:*  
Lee, H. J., Huang, S. Y., Kuo, W. J., Graham, S. J., Chu, Y. H., Stenroos, M., & Lin, F. H. (2020). Concurrent electrophysiological and hemodynamic measurements of evoked neural oscillations in human visual cortex using sparsely interleaved fast fMRI and EEG. *NeuroImage*, 217, 1-13. Article 116910.  
<https://doi.org/10.1016/j.neuroimage.2020.116910>

---

This material is protected by copyright and other intellectual property rights, and duplication or sale of all or part of any of the repository collections is not permitted, except that material may be duplicated by you for your research use or educational purposes in electronic or print form. You must obtain permission for any other use. Electronic or print copies may not be offered, whether for sale or otherwise to anyone who is not an authorised user.



# Concurrent electrophysiological and hemodynamic measurements of evoked neural oscillations in human visual cortex using sparsely interleaved fast fMRI and EEG

Hsin-Ju Lee<sup>a,b,1</sup>, Shu-Yu Huang<sup>c,1</sup>, Wen-Jui Kuo<sup>c</sup>, Simon J. Graham<sup>a,b</sup>, Ying-Hua Chu<sup>a,b</sup>, Matti Stenroos<sup>d</sup>, Fa-Hsuan Lin<sup>a,b,d,\*</sup>

<sup>a</sup> Physical Sciences Platform, Sunnybrook Research Institute, Toronto, Canada

<sup>b</sup> Department of Medical Biophysics, University of Toronto, Toronto, Canada

<sup>c</sup> Institute of Neuroscience, National Yang-Ming University, Taipei, Taiwan

<sup>d</sup> Department of Neuroscience and Biomedical Engineering, Aalto University, Espoo, Finland

## ARTICLE INFO

### Keywords:

Gradient artifact  
Steady-state visual evoked potential  
Fast MRI  
Inverse imaging

## ABSTRACT

Electroencephalography (EEG) concurrently collected with functional magnetic resonance imaging (fMRI) is heavily distorted by the repetitive gradient coil switching during the fMRI acquisition. The performance of the typical template-based gradient artifact suppression method can be suboptimal because the artifact changes over time. Gradient artifact residuals also impede the subsequent suppression of ballistocardiography artifacts.

Here we propose recording continuous EEG with temporally sparse fast fMRI (fast fMRI-EEG) to minimize the EEG artifacts caused by MRI gradient coil switching without significantly compromising the field-of-view and spatiotemporal resolution of fMRI. Using simultaneous multi-slice inverse imaging to achieve whole-brain fMRI with isotropic 5-mm resolution in 0.1 s, and performing these acquisitions once every 2 s, we have 95% of the duty cycle available to record EEG with substantially less gradient artifact. We found that the standard deviation of EEG signals over the entire acquisition period in fast fMRI-EEG was reduced to 54% of that in conventional concurrent echo-planar imaging (EPI) and EEG recordings (EPI-EEG) across participants. When measuring 15-Hz steady-state visual evoked potentials (SSVEPs), the baseline-normalized oscillatory neural response in fast fMRI-EEG was 2.5-fold of that in EPI-EEG. The functional MRI responses associated with the SSVEP delineated by EPI and fast fMRI were similar in the spatial distribution, the elicited waveform, and detection power. Sparsely interleaved fast fMRI-EEG provides high-quality EEG without substantially compromising the quality of fMRI in evoked response measurements, and has the potential utility for applications where the onset of the target stimulus cannot be precisely determined, such as epilepsy.

## 1. Introduction

Electroencephalography (EEG) and functional magnetic resonance imaging (fMRI) can noninvasively record brain activity with millisecond and millimeter resolution, respectively (Huster et al., 2012; Logothetis, 2008; Mulert and Lemieux, 2009). However, EEG and MRI have their respective challenges. Localizing the recorded neural activity by EEG is mathematically ill-posed and coarse (in the range of approximately 6–10 mm), and worsens with the depth from the cortical surface (Niedermeyer and da Silva, 2005; Nunez, 1981; Toga and Mazziotta, 2002). On the

contrary, the hemodynamic responses recorded by fMRI are not directly related to neural activity but instead are the consequence of a complex neurovascular coupling that produces transient changes in cerebral blood flow, cerebral blood volume, and cerebral metabolism of oxygen (Buxton et al., 1998; Logothetis, 2008). To estimate neural activity with high spatiotemporal resolution, EEG and fMRI data can be combined by either (i) estimating the onset and duration of neuronal events by EEG, then using this timing information to identify the areas with fMRI signals related to these events (Laufs et al., 2003; Philiastides and Sajda, 2007; Ullsperger and Debener, 2010); (ii) estimating the areas of significant

\* Corresponding author. Physical Sciences Platform, Sunnybrook Research Institute, Department of Medical Biophysics, University of Toronto, 2075 Bayview Avenue, M4N 3M5, Toronto, Ontario, Canada.

E-mail address: [fhlin@sri.utoronto.ca](mailto:fhlin@sri.utoronto.ca) (F.-H. Lin).

<sup>1</sup> Both contributed equally.

<https://doi.org/10.1016/j.neuroimage.2020.116910>

Received 25 February 2020; Received in revised form 21 April 2020; Accepted 30 April 2020

Available online 7 May 2020

1053-8119/© 2020 The Author(s). Published by Elsevier Inc. This is an open access article under the CC BY-NC-ND license (<http://creativecommons.org/licenses/by-nc-nd/4.0/>).

hemodynamic response by fMRI, then mathematically constraining the neuronal source estimated by EEG to occur within these areas (Babiloni et al., 1998, 2000; Ou et al., 2010); or (iii) jointly estimating neuronal and hemodynamic responses with a modeled relationship between EEG and fMRI data (Riera and Sumiyoshi, 2010; Rosa et al., 2010; Valdes-Sosa et al., 2009).

In each of these cases, EEG and fMRI signals can be recorded separately or concurrently. Concurrent EEG-fMRI recording is preferable when effects related to learning, adaptation, and memory lead to biases in separate recordings (Debener et al., 2006; Ullsperger and Debener, 2010), or when the occurrence of the targeted brain activity cannot be controlled, such as epileptic activity (Gotman et al., 2004; Ives et al., 1993; Krakow et al., 1999b; Seeck et al., 1998). However, the EEG signal recorded concurrently with fMRI is typically heavily distorted (Allen et al., 1998, 2000; Huster et al., 2012; Mulert and Lemieux, 2009; Ullsperger and Debener, 2010). Two most serious EEG artifacts are the gradient artifact (GA (Allen et al., 2000; Mulert and Lemieux, 2009; Wan et al., 2006)) and the pulse artifact (PA (Allen et al., 1998; Huster et al., 2012; Mulert and Lemieux, 2009)). The GA arises from the electromotive force (EMF) on the EEG electrodes induced by the repetitive gradient coil switching during MRI acquisition (Ullsperger and Debener, 2010) and occurs primarily at harmonics of the MRI slice/volume excitation frequency (Mandelkowitz et al., 2006a; Ritter et al., 2008). The PA arises from the EMF on the EEG electrodes induced by the vibration from heartbeats inside an MRI system or the local field change caused by cerebral blood flow (Ullsperger and Debener, 2010). During echo-planar imaging (EPI (Ordidge et al., 1981; Ordidge et al., 1982)) in a 3T MRI system, the GA can be as strong as 3 mV (Ullsperger and Debener, 2010), and the PA is about 200  $\mu$ V (Allen et al., 1998; Huster et al., 2012; Mulert and Lemieux, 2009). In contrast, spontaneous brain waves, such as the alpha rhythm between 8 Hz and 12 Hz, range between 50 and 100  $\mu$ V at the scalp (Berger, 1931). Visual evoked potentials range between 4 and 10  $\mu$ V (Clark et al., 1994; Courchesne et al., 1975; Di Russo et al., 2002; Eason, 1981; Klistorner et al., 1998). Thus, GA and PA are usually far larger than the EEG signals of interest and must be effectively suppressed to present research findings with confidence (Mulert and Lemieux, 2009; Wan et al., 2006).

Data processing methods have been proposed for GA and PA suppression. One common method for GA suppression involves first averaging EEG segments during successive fMRI repetitions to generate a GA “template”, which is then subtracted from the contaminated EEG time-course. However, this average artifact subtraction (AAS (Allen et al., 2000; Niazy et al., 2005)) method has difficulty in suppressing time-varying GA caused by, for example, the movement of the subject (Maziero et al., 2016). Similarly, a PA template can be generated from EEG signals synchronized to the cardiac cycle, and then subtracting the PA template from the contaminated EEG time-course (Niazy et al., 2005). Note that PA suppression is typically performed after GA suppression, because the GA has much higher signal amplitude. Thus, potential GA residuals (incompletely removed GA) can have a deleterious effect on PA suppression (Niazy et al., 2005).

Interleaved EEG-fMRI acquisitions have been proposed to allow high-quality EEG recording in the intervals without fMRI gradient coil switching (Beldzik et al., 2019; Bonmassar et al., 1999, 2001; Goldman et al., 2000, 2002; Kruggel et al., 2000, 2001; Scheeringa et al., 2011, 2016; Uji et al., 2018). Consequently, the shorter the time required for the spatial encoding of the brain volume in the fMRI time series, the more time for EEG without GA. The implementation of interleaved EEG-fMRI requires making a trade-off between MRI spatiotemporal resolution and field-of-view (FOV). With current EPI capabilities, almost the entire repetition time (TR) is crowded with MRI signal excitation and spatial encoding, using the gradient coil switching to meet the prescribed FOV and spatiotemporal resolution. EEG-fMRI is thus contaminated with substantial GA in this case. The difficulty may be overcome, for example, by prescribing fewer slices or by lowering the MRI spatial resolution – each of which reduces the gradient duty cycle (the percentage of time

within each TR interval taken up by gradient coil switching). Neither option is ideal, however, as the chosen slices may miss important brain activity, or image voxels may be too coarse to avoid degrading the detection of the brain activity from partial volume artifacts. Another option is to increase the TR value to reduce the gradient duty cycle without compromising the FOV and spatial resolution, but then the hemodynamic responses to neural activity may not be sampled adequately. Evidently, interleaved EEG-fMRI requires a method of MRI spatial encoding with better spatiotemporal resolution and FOV properties than EPI.

Given the above arguments, the present study was conceived with two goals in mind. The first goal was to assess empirically the performance of GA suppression using AAS. If AAS worked perfectly, then similar oscillatory EEG signals were expected to be observed regardless of the MRI acquisition used. Next, if AAS was not found to work perfectly, then the second goal was to investigate the utility of an alternative concurrent fMRI-EEG acquisition to allow for high-quality EEG measurement of oscillatory brain signals without significantly compromising the fMRI signal sensitivity or spatiotemporal resolution. The alternative acquisition method that was chosen was a version of interleaved EEG-fMRI that involved very fast fMRI spatial encoding, performed only intermittently during continuous EEG to allow for a low gradient duty cycle while preserving the typical TR value for sampling hemodynamic responses. Here, fast fMRI refers to the use of a receiver coil array to accelerate spatial encoding without substantial loss of MRI spatiotemporal resolution. Specifically, simultaneous multi-slice inverse imaging (SMS-InI), a method of sampling the whole brain with 5-mm isotropic resolution in 0.1 s at 3T using a 32-channel head coil array (Hsu et al., 2017), was selected as the proof-of-concept to integrate with concurrent EEG recording. Prescribing SMS-InI with TR = 2 s left 1.9 s (95% of the TR interval) without gradient coil switching, during which EEG data were recorded without GA.

To address both goals, the 15-Hz steady-state visual evoked potential (SSVEP (Bayram et al., 2011; Herrmann, 2001; Norcia et al., 2015)) elicited by visual stimuli flashing at 7.5 Hz, was measured concurrently with EPI or with SMS-InI. Because the 15-Hz SSVEP overlapped with GA in the EPI and EEG combination (EPI-EEG), this enabled an empirical assessment of whether interleaved SMS-InI and EEG (SMS-InI-EEG) improved the quality of SSVEP signals. If GA was suppressed perfectly using AAS, then the SSVEP signal after GA suppression, as acquired either by SMS-InI-EEG or EPI-EEG would be expected to be similar to the SSVEP recorded in the absence of the operation of MRI gradient coils. If GA was not suppressed perfectly, then we hypothesized that the SSVEP at 15 Hz would be better identified from SMS-InI-EEG measurements than from EPI-EEG measurements, as the former lacked overlap between GA and evoked oscillatory neural responses in 95% of the TR interval. Lastly, compared to EPI-EEG, interleaved SMS-InI-EEG was expected to provide high-quality EEG without substantially compromising the quality of fMRI.

## 2. Methods

### 2.1. MRI acquisition

All MRI data were measured on a 3T system (Skyra, Siemens, Munich, Germany) using a 64-channel head-neck receiver coil array with a hole at the back end for routing the EEG cables. Structural images were acquired with the magnetization-prepared rapid gradient echo (MPRAGE) pulse sequence (TR = 2530 ms, echo time TE = 3.03 ms, resolution =  $1 \times 1 \times 1$  mm<sup>3</sup>, FOV = 256 mm, flip angle = 7°, matrix size = 224  $\times$  256, generalized auto-calibrating partial parallel acquisition (GRAPPA) acceleration factor = 2). Functional images were acquired with a SMS-InI sequence (TR/TE = 2000/30 ms, FOV = 210 mm, flip angle = 30°, resolution = 5  $\times$  5  $\times$  5 mm<sup>3</sup>, slice numbers = 24). Spatial encoding was performed in 0.1 s, leaving 1.9 s (95% of the TR interval) free from MRI gradient coil operation. For comparison, T<sub>2</sub>\*-weighted EPI was also

acquired with a typical spatiotemporal resolution (TR/TE = 2000/36 ms, FOV = 224 mm, flip angle = 90°, slice numbers = 30, resolution =  $3.5 \times 3.5 \times 4 \text{ mm}^3$ , GRAPPA acceleration = 2). For EPI, there was 3% of the TR interval (from the end of readouts of the last slice to the onset of magnetization excitation of the first slice) without any spatial encoding. The spatial resolution and the field-of-view in SMS-InI and EPI were chosen to be similar to achieve a fair comparison. The spatial resolution of SMS-InI was limited by the need to sample the whole brain fMRI signal in 0.1 s. On the other hand, the spatial resolution of EPI was slightly higher and reasonably representative of typical applications in the field. We did not lower the spatial resolution of EPI for practical concerns.

## 2.2. EEG acquisition

EEG data were measured using an MRI-compatible system (BrainAmp MR Plus, Brain Products, Gilching, Germany) with a 32-channel EEG cap (BrainCap MR, Brain Products, Gilching, Germany). Electrodes were arranged following the 10–20 international standard. EEG data were referenced with respect to the FCz electrode, with the ground reference taken at the AFz electrode. The electrocardiogram (ECG) was also measured by placing an electrode at the back of the participant.

To ensure high temporal accuracy of the EEG and ECG acquisitions with respect to the MRI acquisitions, the procedure described in (Mandelkew et al., 2006b) was adopted using a frequency divider and phase-locking device as part of the EEG system (BrainAmp MR Plus, Brain Products, Gilching, Germany). The phase-locking device received the 10 MHz transistor-to-transistor logic (TTL) signal from the clock board of the MRI system via a coaxial cable and produced a 5 kHz output signal to synchronize the EEG acquisition. The MRI TR value recorded by the EEG system was confirmed to match the prescribed TR value at the MRI console with an accuracy of 0.2 ms (5 kHz sampling rate). The impedance of each electrode was lower than 9 k $\Omega$  (including the built-in 5 k $\Omega$  impedance) after applying conductive gel. The EEG cap wire bundle was straightened and fixed along the main magnetic field for 50 cm and connected to an EEG amplifier at the rear of the magnet (just outside the bore) to reduce the artifacts generated by the wire (Mullinger et al., 2013). The positions of electrodes over the scalp of a participant were measured by a digitizer (Fastrak, Polhemus, Vermont, USA). These positions were used to register EEG electrodes with the head model derived from structural MRI.

## 2.3. Participants and experiment design

The study received ethics approval from the Institutional Review Board of the National Taiwan University Hospital. Nine healthy young adults provided their free and written informed consent to participate (5 males, all right-handed, corrected to normal vision with contact lenses). Stimulus presentation and behavioral response recording were implemented using E-Prime 2.0 (E-Prime 2.0.10.242 Professional, Psychology Software Tools, Sharpsburg, USA). Participants were instructed to fixate visually on a crosshair at the center of the screen and press a button with their right index finger when the crosshair changed the color from black to red. This task was meant to ensure that participants maintained fixation throughout the EEG-fMRI data acquisition. The red crosshair appeared for 1 s randomly and independently from the onsets of flashing checkerboard patterns (flashing frequency = 7.5 Hz), which were also presented randomly with a minimal inter-stimulus interval of 2 s. The checkerboard subtended 4.3° of visual angle and contained 24 evenly distributed radial wedges with eight concentric rings of equal width. The flashing checkerboard stimuli were used to generate SSVEPs with a primary frequency response at 15 Hz. The choice of studying 15-Hz SSVEPs enabled a direct test of how EEG data were affected by GA suppression using the AAS method, when EPI was performed with slice selection at the same frequency (i.e. 15 Hz = (30 slices)/2 s). Onsets of checkerboard flashing were temporally jittered between 0.2 s and 0.9 s after the beginning of each MRI acquisition of the brain volume to minimize the

effects of GA on EEG data. The same stimulus onset timing was used for concurrent EPI-EEG and for SMS-InI-EEG. In addition, the order of SMS-InI-EEG and EPI-EEG was randomized across participants to avoid potential adaptation effects.

Prior to imaging participants, concurrent SMS-InI-EEG and EPI-EEG were performed of a spherical saline phantom with a mounted EEG cap to characterize GA without PA in the absence of neural activity. Subsequently, three sets of measurements were performed for each participant: EPI-EEG, SMS-InI-EEG, and EEG recorded inside the MRI system but with no imaging (inside-MRI). Three runs of data were collected for each measurement, with each run lasting 8 minutes. Fifty flashing checkerboard trials were presented to a participant in each run. To compare the estimated radiofrequency power deposition for SMS-InI and EPI data collection, the average specific absorption rate (SAR) values estimated by the MRI system were recorded throughout.

## 2.4. EEG analysis

The EEG processing was implemented in MATLAB (Mathworks, Natick, MA, U.S.A). For EPI-EEG and SMS-InI-EEG, these procedures included GA suppression by average artifact subtraction (AAS) (Allen et al., 2000). To account for the timing difference in the clock accuracy between MRI (10 MHz) and EEG (5 kHz) systems, further alignment between the gradient artifact template and the EEG data was achieved by interpolating with an accuracy of 0.2, 0.02, 0.002 and 0.0002 samples in four iterations to achieve the numerical sampling rate of 0.025 MHz, 0.25 MHz, 2.5 MHz, and 25 MHz, respectively. The GA template was dynamically estimated over seven TR intervals. Estimating the GA template by averaging over a small number of TR intervals may leave neural signals in the artifact template and confound the results (Steyrl and Muller-Putz, 2019). To study this issue, we parametrically varied the number of averages between 7, 14, and 28 TR intervals to estimate a GA template in windows of 14 s, 28 s, and 56 s, respectively. EEG data were further zero-phase band-pass filtered between 1 Hz and 50 Hz, down-sampled to 500 Hz, followed by the detection of cardiac R-peaks, PA suppression by the optimal basis set (OBS) method (Niazy et al., 2005), and removal of the average time series across electrodes. Note that the GA templates were separately modeled for SMS-InI and EPI scans. For the EEG data collected in the inside-MRI condition, the same procedures were followed except that GA suppression by AAS was not undertaken. Oscillatory features in the EEG signal were quantified using the Morlet wavelet transform with the central frequency varying between 5 Hz and 80 Hz. The temporal window was 5 cycles for each central frequency.

SSVEPs were calculated by first extracting EEG signals between 200 ms before and 1000 ms after the onset of each visual stimulus for all trials of a given measurement (EPI-EEG, SMS-InI-EEG, and inside-MRI). The constant and the linear drift in each of these EEG trials were then removed by linear regression. Trials with a maximum EEG signal >700  $\mu\text{V}$  were excluded. The SSVEPs were then derived by averaging across trials at each electrode. The sources of SSVEPs were estimated by distributed source modeling based on a realistic head model (Lin et al., 2006). Specifically, the  $T_1$ -weighted MPRAGE MRI data were used to create scalp, skull, and brain models using FreeSurfer (<https://surfer.nmr.mgh.harvard.edu>). Potential EEG source locations at the gray and white matter boundary were identified with approximately 5-mm separation between the nearest neighboring source locations. The locations of EEG electrodes were manually registered to the scalp model. A forward matrix accounting for the modeled EEG signals elicited by each current dipole across all electrodes was created using the Helsinki boundary element method (BEM) framework for MEG/EEG (Stenroos et al., 2007; Stenroos and Nummenmaa, 2016). Three orthogonal current dipoles were modeled at each source location. The EEG current source was determined using the minimum-norm estimate method (Lin et al., 2006) without constraining the current dipole orientation. The estimated current density distributions were then transformed to the Montreal

Neurological Institute (MNI) coordinate system for group-level averaging. Finally, the significance of the estimated neural currents generating the SSVEP was calculated using dynamic statistical parametric maps (Dale et al., 2000), where the values at each brain location at each time instant were calculated by first subtracting the average of the baseline interval and then dividing by the standard deviation of the baseline interval to give Z-scores.

## 2.5. Functional MRI analysis

The SMS-InI data were reconstructed to obtain one brain volume image per 0.1 s (Hsu et al., 2017). The first three brain volumes in each run of SMS-InI and EPI were excluded to ensure that the magnetization reached a steady state. The time series of SMS-InI brain volumes was motion-corrected, spatially smoothed (3D Gaussian kernel with full-width-half-maximum, FWHM, of 5 mm) co-registered to the high spatial resolution brain anatomy of the participant, and transformed to the MNI coordinate system. EPI data were motion-corrected, slice-timing

corrected, spatially smoothed in analogous fashion to the SMS-InI data (3D Gaussian kernel with FWHM of 5 mm), co-registered to the high spatial resolution brain anatomy of the participant, and transformed to the MNI coordinate system.

The fMRI signals elicited by the checkerboard flashing were estimated by the General Linear Model (GLM). Specifically, a modeled fMRI time series was built by convolving a finite impulse response function (30-s duration; 6-s pre-stimulus baseline). Confounds of linear drift, run-specific signal shift, head motion, and the average of instantaneous fMRI signals across the whole brain were included in the GLM to model nuisance effects. The significance of the hemodynamic responses was quantified by the Z-score with respect to the baseline fluctuation. The  $p$ -values were corrected for multiple comparisons using the Bonferroni method. The spatial overlap of significant fMRI signals, between maps generated by EPI and SMS-InI, was calculated using the Jaccard index (Jaccard, 1901). It was hypothesized that the simple checkerboard flashing elicited significant fMRI signals at the primary and secondary visual cortices, both of which were defined anatomically by FreeSurfer.

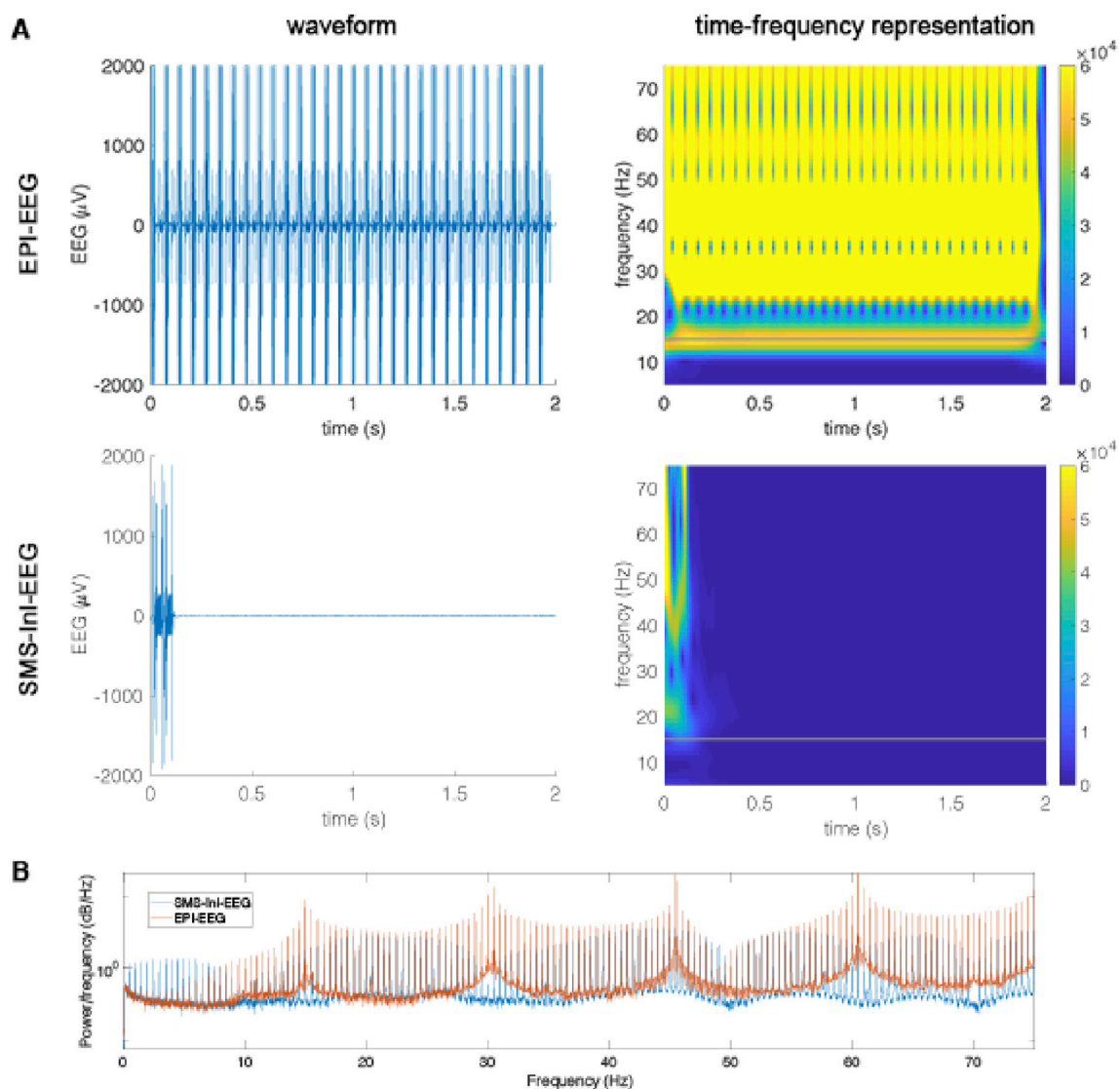


**Fig. 1.** Results of the phantom experiment. A: EEG waveforms at the Oz electrode (left column) and the associated time-frequency representations (right column) using EPI-EEG (top row) and SMS-InI-EEG (bottom row). Time zero indicates the onset of the acquisition of an MRI volume. The gradient artifact (GA) persisted continuously over the repetition time (TR) interval of 2 s during EPI-EEG, whereas GA was restricted to the first 0.1 s during SMS-InI-EEG. The gray horizontal lines in the time-frequency representations indicate 15 Hz, the frequency of the expected steady-state visual evoked potential in this study. B: Power spectral density plots of the same waveforms from EPI-EEG and SMS-InI-EEG. Patterns of discrete frequencies at multiples of the inverse of TR were found. SMS-InI-EEG had lower power than EPI-EEG at the fundamental (15 Hz) and all harmonic frequencies of the SSVEP.

The detection of fMRI signals was quantified by calculating the area-under-curve (AUC) value using receiver operating characteristic (ROC) analysis (Fawcett, 2006).

### 3. Results

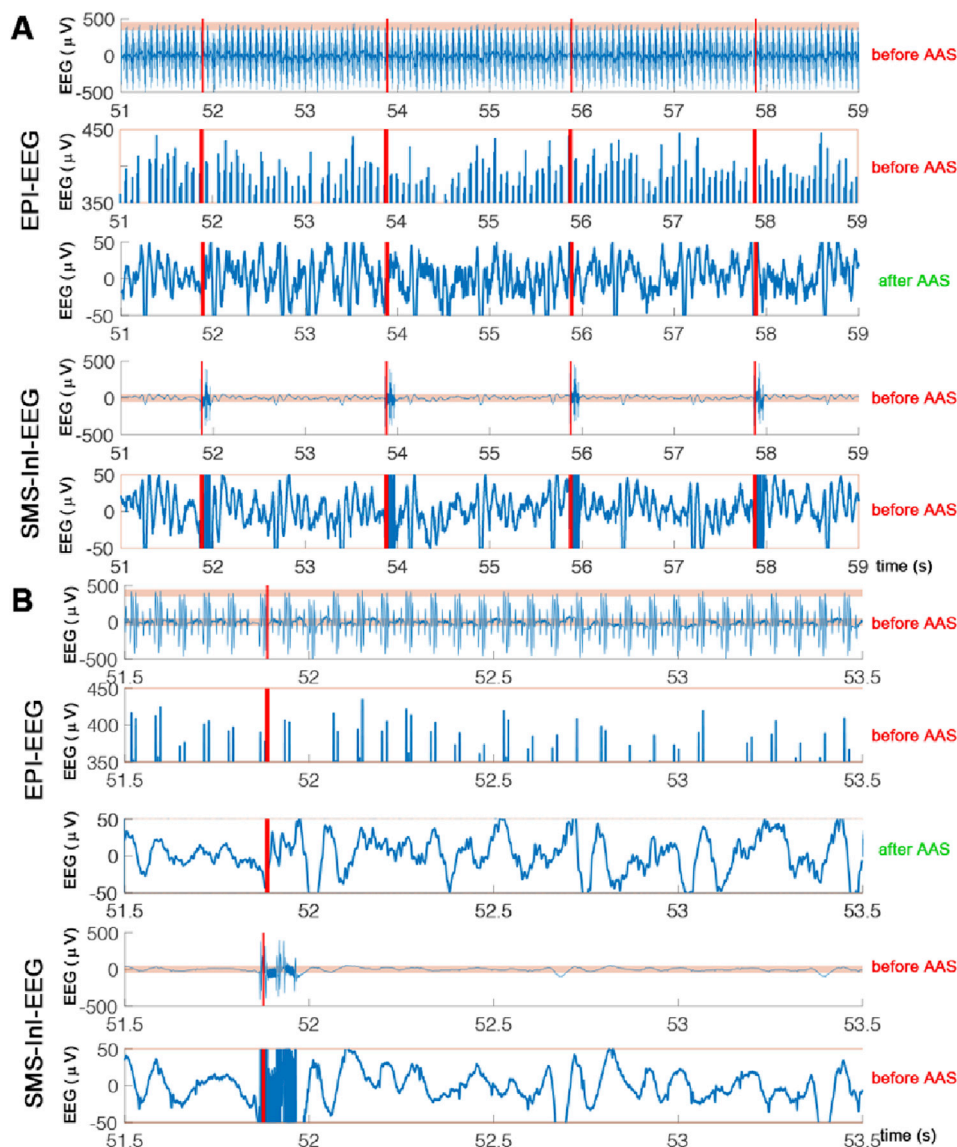
As an initial safety check, the SAR values for EPI-EEG were between 0.12 and 0.13 W/kg across participants. For SMS-InI-EEG, the analogous values were between 0.09 and 0.10 W/kg, respectively. Considering that EPI-EEG was within the safety limit, the lower SAR values for SMS-InI-EEG suggested that any potential concern about radiofrequency heating hazard was relatively small for this imaging method.

Fig. 1 shows the temporal waveforms of the EEG signal at the Oz electrode using EPI-EEG and SMS-InI-EEG in the phantom measurement. Strong and consistent GAs were observed on EEG in EPI-EEG over the 2-s TR interval. Conversely, the voltage induced by SMS-InI-EEG on the electrode was limited to the first 0.1 s of the TR interval. The time-frequency representations (TFRs) of these EEG signals are also shown in Fig. 1. Strong oscillatory signals were observed in EPI-EEG at two frequency ranges: approximately 15 Hz and above 30 Hz. Strong oscillatory EEG signals were also observed for SMS-InI-EEG, although they were restricted to the first 0.1 s of the TR interval, and at frequencies

above 15 Hz. These data confirm that the induced EEG signals by SMS-InI were spectro-temporally restricted, providing the opportunity for improved recording of the EEG signals of interest by minimizing the GA interference from MRI. Last, the power spectral density plots of the EEG signals from both EPI-EEG and SMS-InI-EEG are also shown in Fig. 1. Patterns of discrete frequencies at multiples of the inverse of TR were found, similar to a previous study (Mandelkowitz et al., 2010). Importantly, SMS-InI-EEG had lower power than EPI-EEG at the fundamental (15 Hz) and all harmonic frequencies of the SSVEP.

Segments of EEG recordings at the Oz electrode from a representative participant are shown in Fig. 2. Similar to the phantom measurement, strong and continuous GA ranging between  $-500$  and  $+500$   $\mu\text{V}$  was observed for EPI-EEG, throughout each TR interval. Examining the EEG signals in the 100  $\mu\text{V}$  range between  $+350$  and  $+450$   $\mu\text{V}$ , the GA was observed to fluctuate as a function of time with considerable variability. After GA suppression by AAS, a waveform with clear PA including the neural signal was observed in EPI-EEG in the range between  $-50$  and  $+50$   $\mu\text{V}$ . In contrast, SMS-InI-EEG showed large GA signals only within the first 0.1 s of each TR interval. At all other times, typical quasi-periodic PA was observed in MRI-quiet periods within the 100  $\mu\text{V}$  range between  $-50$  and  $+50$   $\mu\text{V}$ , even before GA suppression.

To compare SMS-InI-EEG and EPI-EEG results with different stages of



**Fig. 2.** Representative raw EEG signals at the Oz electrode for EPI-EEG (the top three rows) and SMS-InI-EEG (the fourth and the bottom rows) over four TR intervals (A) and one TR interval (B). EPI induced strong gradient artifact (GA) in the EEG recordings (top row). On further examination of the EEG signal content ranging from  $+350$  to  $+450$   $\mu\text{V}$  (second row), fluctuations were observed without clearly repetitive patterns over time. Clear pulse artifacts were observed after GA suppression in EPI-EEG in the range between  $-50$  and  $+50$   $\mu\text{V}$  (third row). In contrast, without GA suppression, SMS-InI-EEG had strong GA only within the first 0.1-s of each TR interval (fourth row). The EEG signals fluctuated between approximately  $-50$  and  $+50$   $\mu\text{V}$  for the rest of the time, including quasi-periodic pulse artifact.

signal processing, Fig. 3 shows the temporal standard deviation of EEG signals at each electrode after GA suppression, and after GA and PA suppression, from a representative participant and from all participants. The EEG signals from SMS-InI-EEG had a smaller standard deviation at all electrodes than those from EPI-EEG. For a representative participant (Fig. 3 top row), the standard deviation of the EEG signals from EPI-EEG and SMS-InI-EEG averaged across all electrodes was  $27.8 \pm 11.3 \mu\text{V}$  and  $18.4 \pm 8.5 \mu\text{V}$ , respectively, after GA suppression. The standard deviation of EEG signals in SMS-InI-EEG was 66% of that observed in EPI-EEG. After both GA and PA suppression, the standard deviations of the EEG signals in EPI-EEG and SMS-InI-EEG were  $22.3 \pm 11.2 \mu\text{V}$  and  $15.4 \pm 7.6 \mu\text{V}$ , respectively. In this case, the standard deviation of EEG signals in SMS-InI-EEG was 69% of that observed in EPI-EEG.

The temporal standard deviation of EEG signals was also examined across electrodes from all participants (Fig. 3 bottom row). After GA suppression only, the average standard deviation of the EEG signals from SMS-InI-EEG was 68% ( $18.5 \pm 8.5 \mu\text{V}$ ) of that from EPI-EEG ( $27.2 \pm 11.0 \mu\text{V}$ ). After both GA and PA suppression, the average standard deviation of the EEG signals in SMS-InI-EEG was 54% ( $11.9 \pm 5.4 \mu\text{V}$ ) of that in EPI-EEG ( $21.0 \pm 8.1 \mu\text{V}$ ). Furthermore, statistical testing revealed that the standard deviation of the EEG signals from SMS-InI-EEG was significantly smaller than that from EPI-EEG, either after GA suppression alone, or after both GA and PA suppression (Wilcoxon rank sum test;  $p = 8.9 \times 10^{-7}$  and  $3.4 \times 10^{-7}$ , respectively).

Single trial responses at electrodes O1 and O2 are shown in Fig. 4 for SMS-InI-EEG and EPI-EEG of two representative participants. For both participants, the EPI-EEG responses exhibited either very positive or very negative evoked potentials without a discernable oscillatory pattern around 15 Hz. In contrast, visual inspection of the SMS-InI-EEG responses showed some evidence of 15 Hz oscillations across the trials. As the signal-to-noise ratio (SNR) for single-trial EEG can be low, we also calculated the average time course across all the trials and runs (right column in Fig. 4), comparing the results for SMS-InI-EEG, EPI-EEG, and the EEG data collected during the “inside MRI” condition. Additionally, we calculated the statistical significance of the 15-Hz oscillation in the average waveforms after the stimulus onset. The similarity of the average waveforms between SMS-InI-EEG and the “inside MRI” condition was found to be higher than that between EPI-EEG and the “inside MRI” condition. The time-frequency plots suggested that the 15-Hz oscillations were more significant in SMS-InI-EEG than in EPI-EEG between 0.1 s and 1 s after the stimulus onset. These oscillations in SMS-InI-EEG were more similar to those in the “inside MRI” condition than were the oscillations in EPI-EEG.

Fig. 5 shows source localization Z-score maps of the significance of the estimated 15-Hz neural currents averaged between 300 ms and 1100 ms after the visual stimulus onset. The significance level was calculated with respect to the 15-Hz oscillation in the 200 ms pre-stimulus interval.

Strong 15-Hz SSVEP sources were observed in the occipital lobe in the visual cortex for SMS-InI-EEG, whereas the results were weaker and less well localized for EPI-EEG.

Fig. 6 shows the average significance of the 15-Hz neural oscillations between 300 ms and 1100 ms after the stimulus onset in SMS-InI-EEG with the GA template estimated from a window of 7 TR intervals; and in EPI-EEG with the GA template estimated from a window of 7, 14, and 28 TR intervals on the same two representative participants shown in Fig. 4. Suppressing the GA in EPI-EEG using artifact templates estimated across a window of 7, 14, or 28 TR intervals provided less significant 15-Hz neural oscillations at the visual cortex than SMS-InI-EEG using an artifact template estimated across a window of 7 TR intervals. The potentially spurious 15-Hz oscillations outside the visual cortex were less in SMS-InI-EEG than in EPI-EEG, regardless of the template window size used in the latter analysis. The suppression of GA did not improve much for EPI-EEG when the template window size was expanded. These results excluded the possibility that the limited performance in estimating SSVEP using EPI-EEG was due to the GA template waveforms containing neural responses.

Fig. 7 shows the estimated neural currents using source modeling from the group average at the visual cortex for the EPI-EEG, SMS-InI-EEG, and inside-MRI conditions. The estimated neural currents were first averaged across participants, then the size of the averaged evoked potential was divided by the standard deviation of the averaged evoked potential in the pre-stimulus interval for reporting purposes. In all cases, a transient visual evoked potential was first observed with a peak signal amplitude at approximately 170 ms after the onset of the visual stimulus, followed by oscillatory visual evoked potentials (VEPs) thereafter during the time interval between approximately +300 ms to +1100 ms. After normalizing the oscillatory VEP with respect to the temporal standard deviation of the baseline interval (Fig. 7 A), the inside-MRI condition produced the transient response with the highest Z score ( $Z = 58$ ), whereas the analogous values for SMS-InI-EEG and EPI-EEG were 23 and 15, respectively. On visual inspection, the sustained 15-Hz oscillatory patterns were more easily distinguished for inside-MRI and SMS-InI-EEG than they were for EPI-EEG. Taking the peak of the transient response as a physiological marker, the SSVEP Z-score waveform was subsequently scaled to unity across the three conditions (Fig. 7 B). After scaling, the oscillatory patterns were similar and prominent for inside-MRI and SMS-InI-EEG, whereas EPI-EEG resulted in oscillations that were harder to observe.

Fig. 8 shows the TFRs of the estimated neural currents at the visual cortex using group-averaged data acquired by inside-MRI, SMS-InI-EEG, and EPI-EEG. The significance of these TFRs was quantified with respect to the standard deviation of the oscillatory signal in the baseline interval to yield Z scores, and then color-coded for display purposes. Clear SSVEP oscillation at 15 Hz was observed between approximately +300 ms to

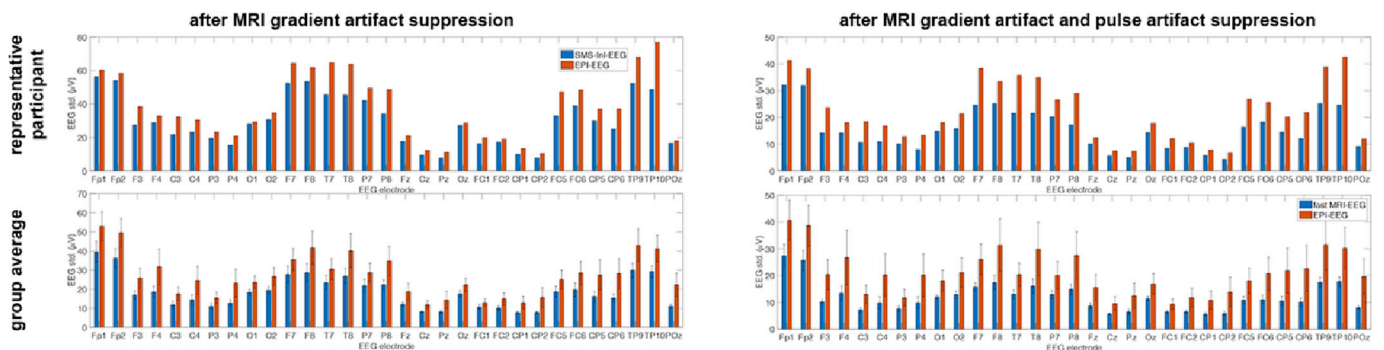
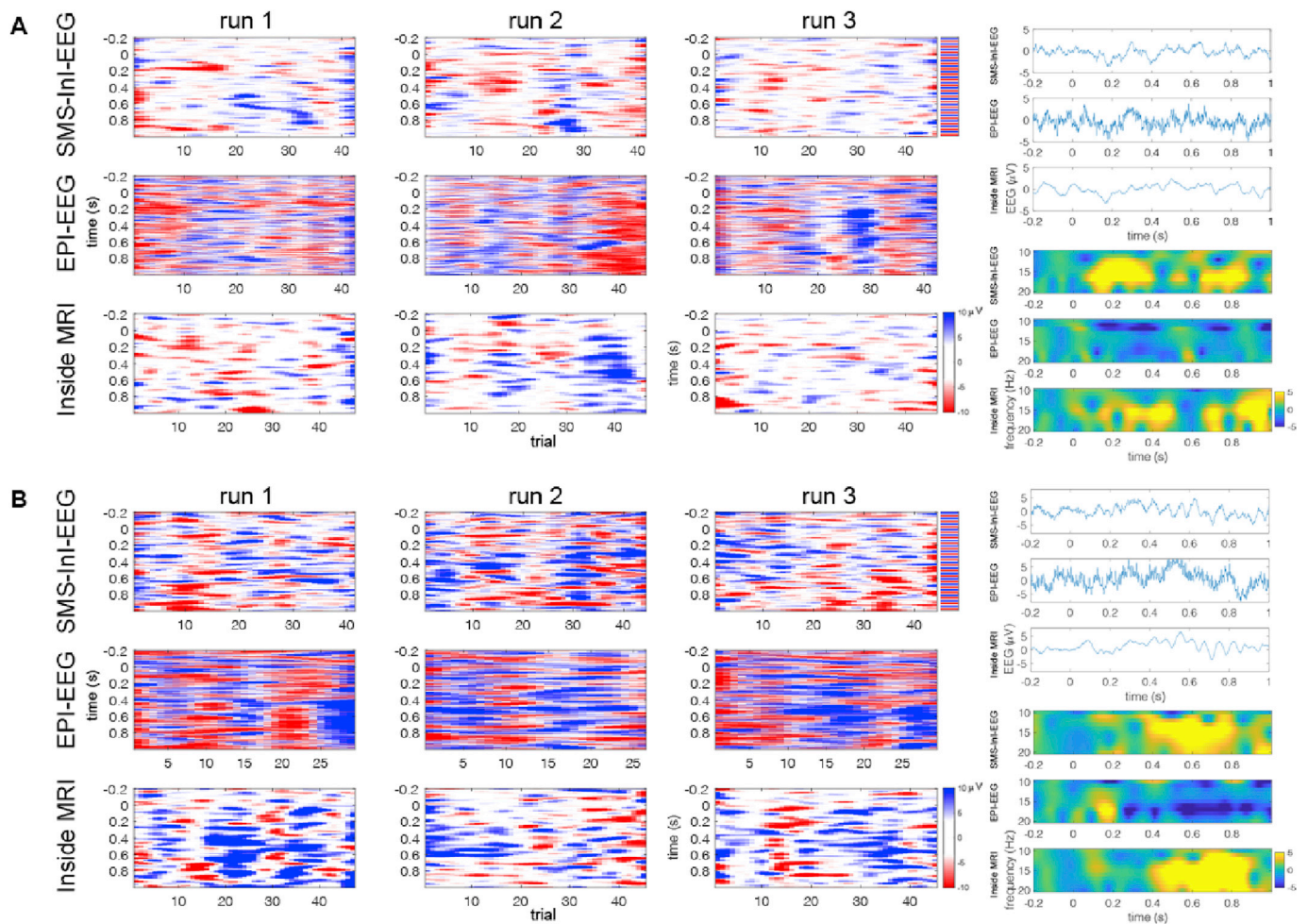
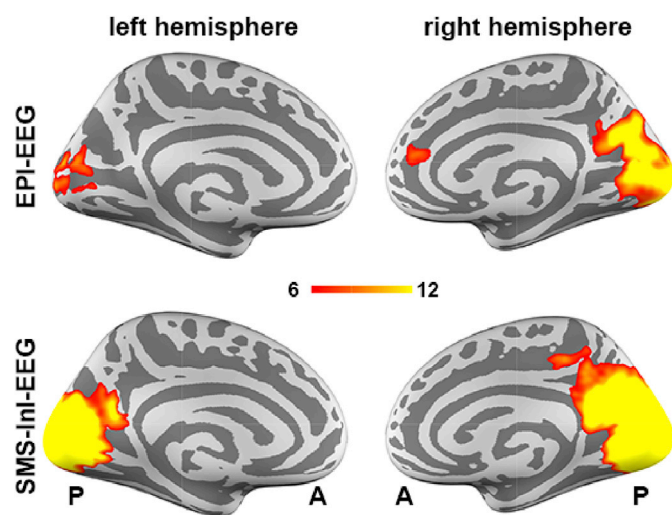


Fig. 3. The temporal standard deviation (std.) of the EEG signals at different electrodes from EPI-EEG and SMS-InI-EEG of a representative participant (top row) and across all participants (bottom row). These standard deviations were calculated separately either after gradient artifact suppression (left column) or after both gradient and pulse artifact suppression (right column). All electrodes showed a higher standard deviation of EEG signals from EPI-EEG than from SMS-InI-EEG. The error bars represent the standard deviation across participants.



**Fig. 4.** Single trial responses at electrode O1 (A) and O2 (B) from two representative participants, for SMS-InI-EEG and EPI-EEG. A 15-Hz oscillatory pattern was shown at the top right corner of each panel for comparison. The right-most column (top) consists of the EEG signal time-courses averaged across trials and runs in SMS-InI-EEG, EPI-EEG, and the “inside MRI” condition during which EEG signals were collected without any MRI acquisitions. Time-frequency plots of the average EEG waveforms are also shown in the right-most column (bottom). Both SMS-InI-EEG and “inside MRI” provided more prominent 15-Hz oscillations than EPI-EEG.



**Fig. 5.** Source localizations of the 15-Hz SSVEP averaged between 300 ms and 1100 ms after the visual stimulus onset using SMS-InI-EEG and EPI-EEG. Strong 15-Hz SSVEP was observed in SMS-InI-EEG in the occipital lobe in the visual cortex. Colors code the average (between 300 ms and 1100 ms after the stimulus onset) Z-score with respect to the 15-Hz oscillation in the pre-stimulus baseline. A: anterior. P: posterior.

+1100 ms for inside-MRI and SMS-InI acquisitions, whereas the oscillation was much less for EEG-EPI. The 15-Hz SSVEP after normalizing to the baseline oscillation was  $8.5 \pm 2.2$ ,  $10.6 \pm 2.6$ , and  $4.3 \pm 2.3$  for inside-MRI, SMS-InI-EEG, and EPI-EEG, respectively. Compared to EPI-EEG (4.3), the baseline-normalized 15-Hz SSVEP measured with SMS-InI-EEG (10.6) was 2.5-fold ( $p < 10^{-20}$ ; Wilcoxon rank sum test for equal medians) of that with EPI-EEG (4.3).

Regarding the fMRI results, as shown in Fig. 9, both EPI and SMS-InI detected significant hemodynamic responses in the visual cortex ( $Z \geq 5$ ;  $p = 0.006$  after Bonferroni correction for multiple comparisons) due to the flashing checkerboard stimuli. The Jaccard index of overlapping spatial response was 0.55 for the two imaging methods. In both cases, the hemodynamic response was located in an area that matched the anatomically defined primary and secondary visual cortex (Jaccard index: 0.55 and 0.45, respectively). Taking anatomically defined primary and secondary visual cortex as the area generating the hemodynamic response, the sensitivity and specificity of detecting hemodynamic responses by either fMRI acquisition were quantified by the AUC using the ROC analysis. The AUC values were 0.95 and 0.96 for EPI-EEG and SMS-InI-EEG, respectively. The hemodynamic response waveforms at the visual cortex with jointly significant activity, as detected by SMS-InI and EPI, were also similar (Fig. 10). Together, these results suggest that EPI and SMS-InI had very similar spatiotemporal sensitivity for detecting hemodynamic responses in this fMRI-EEG experiment.

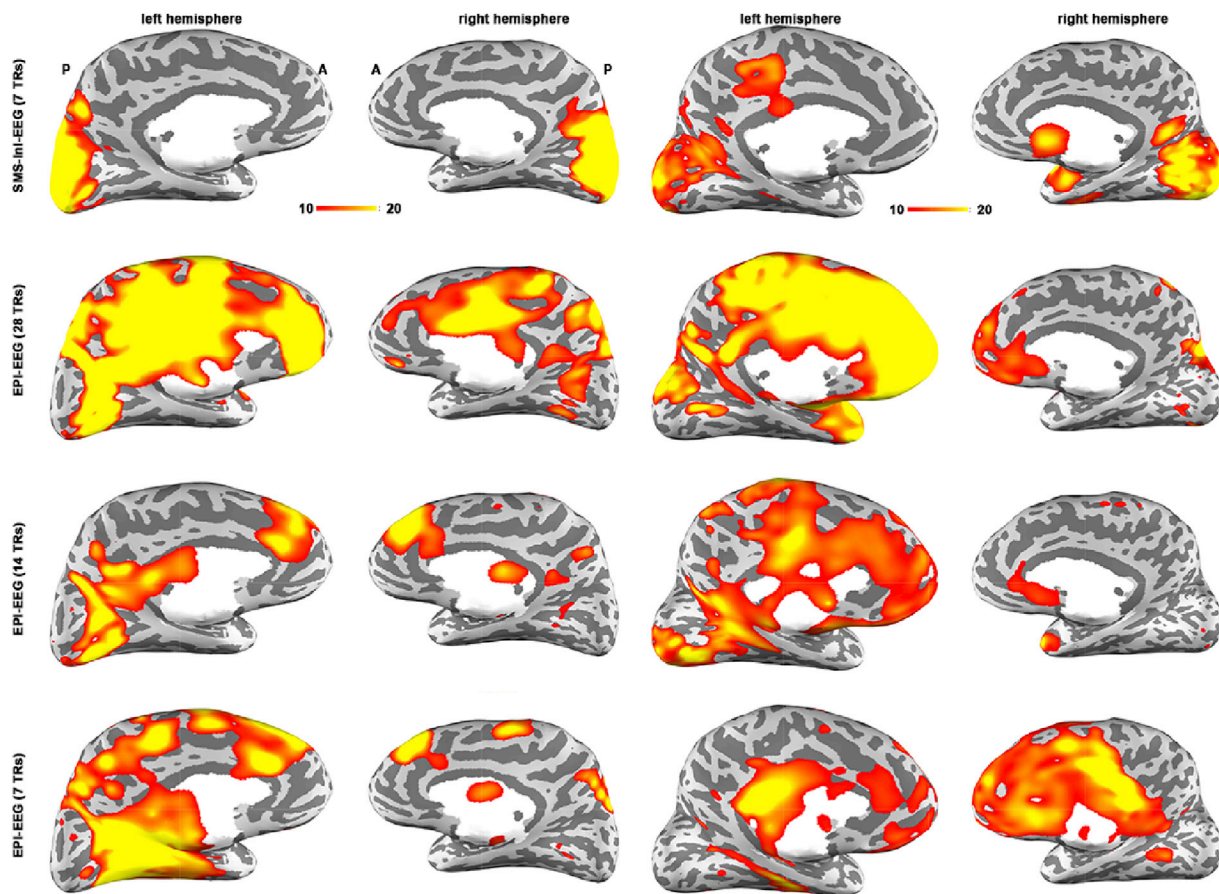


**Fig. 6.** Source localizations of the 15-Hz SSVEP averaged between 300 ms and 1100 ms after the visual stimulus onset using SMS-InI-EEG and EPI-EEG, for the same two participants reported in Fig. 4. The gradient artifact in EPI-EEG was suppressed by artifact templates estimated from a window of 7, 14, and 28 TR intervals in 14 s, 28 s, and 56 s, respectively. The gradient artifact in SMS-InI-EEG was suppressed by an artifact template estimated from a window of 7 TR intervals. A strong source of 15-Hz SSVEP was observed in SMS-InI-EEG in the occipital lobe in the visual cortex. EEG-EPI provided reduced 15-Hz SSVEP in the visual cortex and potentially spurious 15-Hz responses outside the visual cortex. Colors code the average (between 300 ms and 1100 ms after the stimulus onset) Z-score with respect to the 15-Hz oscillation in the pre-stimulus baseline. A: anterior. P: posterior.

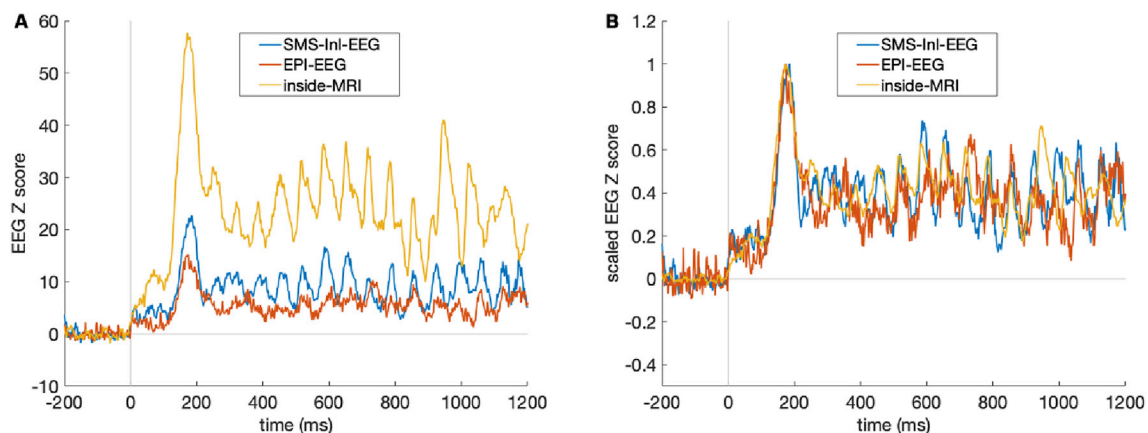


**Fig. 7.** The steady-state visual evoked potential (SSVEP) at the visual cortex in SMS-InI-EEG, EPI-EEG, and inside-MRI. A: Z-scores produced when the 15-Hz oscillatory VEP was normalized to the temporal standard deviation of the baseline period (−200 ms to 0). More prominent oscillatory waveforms were observed for inside-MRI and SMS-InI-EEG than for EPI-EEG. B: EEG time courses subsequently scaled such that the transient peak at approximately 180 ms was 1.0 in each condition. In this case, the oscillatory waveforms for inside-MRI and SMS-InI-EEG were quite similar, whereas the oscillation was less clear for EPI-EEG.

#### 4. Discussion

Sparsely interleaved EPI-EEG has been introduced previously to reduce contamination in the EEG signals directly as they are recorded by limiting MRI-induced artifacts (Beldzik et al., 2019; Bonmassar et al.,

1999, 2001; Goldman et al., 2000, 2002; Kruggel et al., 2000, 2001; Scheeringa et al., 2011, 2016). More recently, concurrent multiband EPI-EEG (Uji et al., 2018) has been used to allocate 75% of the TR interval (2.25 s in a TR value of 3 s) to sample EEG signals without GA and to permit fMRI at 3-mm isotropic resolution. Here, SMS-InI-EEG was

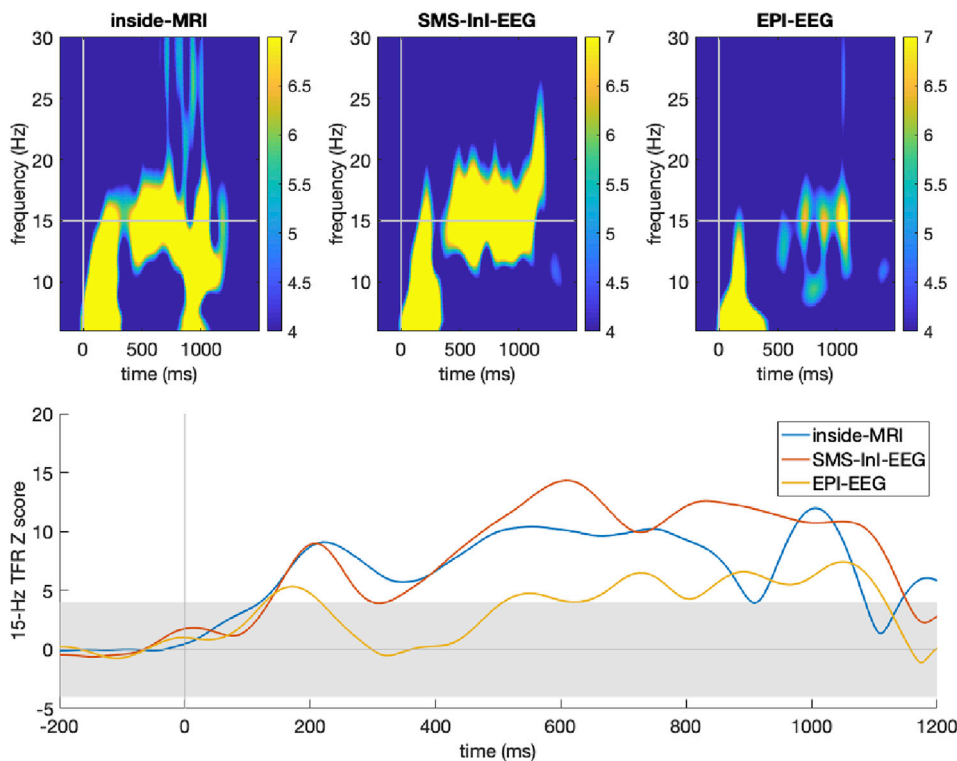


Fig. 8. Top row: baseline-normalized time-frequency representation of the SSVEP from EPI-EEG, SMS-InI-EEG, and inside-MRI. Oscillatory SSVEP at 15 Hz was strongly evident between +300 ms and +1100 ms after the visual stimulus onset for both inside-MRI and SMS-InI-EEG, but was much reduced for EEG-EPI. Bottom row: The Z-score time-courses of the baseline-normalized oscillatory power at 15 Hz. The gray horizontal bar indicates bounds of the magnitude Z-score < 4 (uncorrected  $p < 6 \times 10^{-5}$ ).

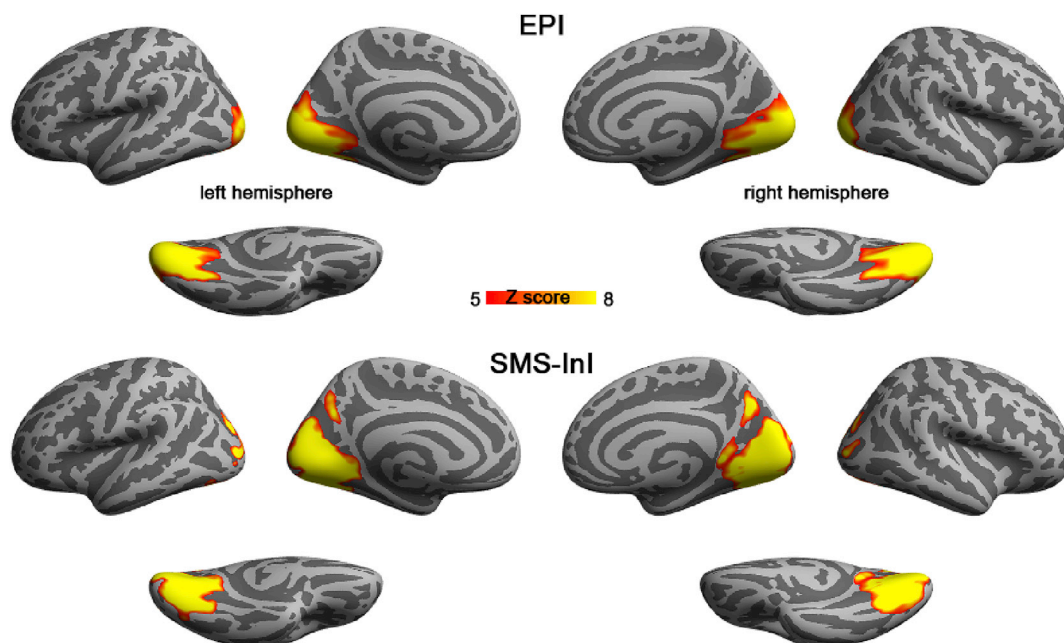
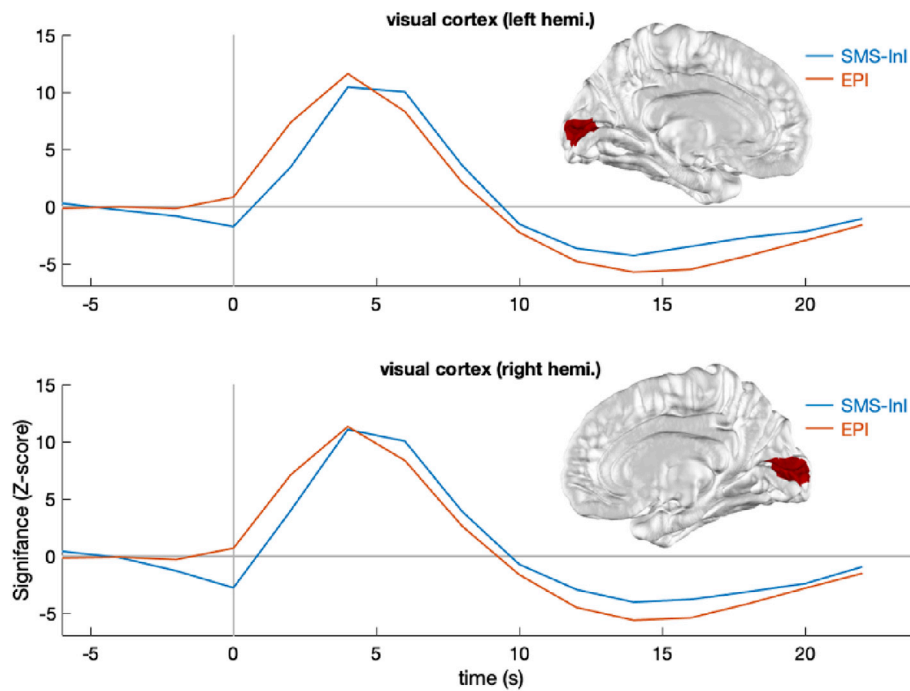


Fig. 9. Significant fMRI signals at the visual cortex elicited by 7.5-Hz checkerboard flashing were observed for EPI and SMS-InI.

proposed as a useful alternative, providing 95% of the TR interval to acquire high-quality EEG results with low levels of artifacts, while providing fMRI with 5 mm isotropic resolution at TR = 2 s with similar sensitivity as that obtained with conventional EPI. Across participants, the average standard deviation of EEG signals achieved across all electrodes with SMS-InI-EEG was 54% of that achieved with EPI-EEG (Fig. 3). The observed SSVEP consisted of a transient response with its peak at approximately 180 ms and a sustained oscillatory response between 300 ms and 1100 ms after the stimulus onset, in agreement with previous SSVEP findings (Norcias et al., 2015; Zhang et al., 2018).

Importantly in the present work, the dominant frequency of the SSVEP was chosen specifically to coincide with the dominant frequency of the GA in EPI-EEG (the ratio between the number of slices and the TR value). This choice was meant to test whether GA suppression works without degrading physiologically-related EEG features. Although EPI acquisition parameters can in principle be chosen so that the spectral components of GA have less overlap with the EEG frequencies of interest, this approach can be limiting when the frequencies of interest are not well known or evolve during the experiment. Thus, it is of interest to develop an alternative MRI acquisition strategy that overcomes these



**Fig. 10.** Z-score waveforms of the hemodynamic responses at the visual cortex (top row: left hemisphere; bottom row: right hemisphere) for jointly significant activity as detected by EPI and SMS-InI (the dark red region in the figure inset).

limitations. By studying the “worst-case scenario”, in which EEG and GA frequency components overlapped strongly, we tested empirically whether SMS-InI-EEG could selectively suppress GA without degrading the detection of the expected oscillatory brain responses. Smaller variability of EEG signals (Figs. 1–3) and more prominent 15-Hz SSVEP in SMS-InI-EEG than in EPI-EEG suggested the limitation of GA suppression by AAS. These results also corroborate previous studies, which suggested that GA is a primary problem for studying high frequency oscillatory activity, with residual GA easily obscuring the small amplitude neuronal signal of interest even after attempted correction (Mullinger et al., 2008, 2011). A possible reason why a gradient template cannot satisfactorily suppress GA is the confounding effect of head motion, which perturbs the orientation of the electrodes in relation to the applied gradient fields in a non-periodic manner. The associated significant fMRI signals were very similar between SMS-InI-EEG and EPI-EEG in their spatial distributions and the elicited waveforms (Figs. 8 and 9). Collectively, these results provide strong evidence that i) the performance of the current practice of GA suppression using AAS is imperfect; and ii) in comparison to conventional EPI-EEG, sparsely interleaved fast fMRI-EEG can provide enhanced EEG quality and similar fMRI signal sensitivity and spatio-temporal resolution.

The PA and GA exist in different frequency bands, and their occurrences are not synchronized (Allen et al., 1998, 2000; Niazy et al., 2005). Thus, during EPI-EEG, the residual GA after AAS remained in the EEG recordings and affected the performance of subsequent PA suppression. Considering that the residual GA is caused by mismatch between the artifact template and the actual time dependence of the artifact, it is logical that residual GA is more problematic for concurrent EEG and fMRI as the duty cycle of gradient coil switching increases. This is consistent with the findings of higher EEG SNR for inside-MRI than for SMS-InI-EEG; and higher EEG SNR for SMS-InI-EEG than for EPI-EEG (Figs. 1–3).

In this study, we focused on the potential benefit of interleaved fast fMRI-EEG to the detection of the 15-Hz SSVEP. The GA in EPI-EEG was not only strong at a band around 15 Hz, but also between 30 Hz and 80 Hz. In contrast, the GA for SMS-InI-EEG was markedly lower over 95% of the TR interval (Fig. 1). Thus, it is anticipated that fast fMRI-EEG

methods can also be used to improve the sensitivity and specificity of electrophysiological features at beta (Hari and Salmelin, 1997) and gamma (Buzsaki and Wang, 2012) bands.

It might be speculated that there was no need to perform GA correction in SMS-InI-EEG, because GA artifacts were absent for 95% of each TR interval. However, to suppress PA, EEG waveforms need to be segmented and temporally aligned (with respect to ECG QRS peaks in this study) before using the OBS method. Without GA suppression, the segmented and aligned EEG waveforms in SMS-InI-EEG would have brief but strong GA at different phases of heartbeats, which occurred asynchronously within each TR interval. The durations of the expected evoked responses, PA, and GA due to stimuli, heart beats, and MRI acquisitions were about 1 s, 1 s (Niazy et al., 2005), and 0.1 s (for SMS-InI), respectively. Therefore, in suppressing the PA using the OBS method, we had to prepare EEG data matrices by aligning EEG signals across R peaks with the duration of a few hundreds of milliseconds before and after each R peak. Principal Component Analysis cannot be applied to such EEG data matrices by “ignoring” the GA in the 100-ms interval. Thus, the GA must be first removed by AAS to allow for normal PA suppression, even though the EEG data were sampled with SMS-InI.

This study chose SMS-InI (Hsu et al., 2017) as the fast MRI acquisition method, although other options are available, such as SMS-EPI (Setsonpop et al., 2012). SMS-InI differs from SMS-EPI by including simultaneous echo-refocusing (Chen et al., 2015b; Feinberg and Setsompop, 2013) in the spatial encoding, and a regularized image reconstruction. When operating at the 10-Hz sampling rate, the time-domain SNR of SMS-InI (30) is 50% higher than SMS-EPI (20) (Chen et al., 2015a, 2015b; Zhu et al., 2016), which is why the former was used in the present work. Future advancement of fast MRI for higher spatial resolution, shorter imaging acquisition time, and higher fMRI signal sensitivity would be useful to replace SMS-InI to obtain even better EEG and fMRI. As indicated by Fig. 6 in particular, there is still some scope to improve EEG signals during concurrent fMRI, toward signal characteristics that match those obtained when fMRI is absent.

One limitation of using SMS-InI is that the method has a relatively low nominal spatial resolution (5 mm), which initially may seem insufficient for fMRI. However, images are typically spatially smoothed in very many

fMRI experiments, using a Gaussian kernel with a FWHM set at approximately this resolution. It has been suggested that smoothing data with 8 mm FWHM was optimal for group inferences (Mikl et al., 2008). We may choose to improve the resolution of SMS-InI by increasing the data acquisition time. The trade-off here would be reduction of time available within each TR interval for EEG signals without MRI artifacts.

The EPI in this study had a spatial resolution of about 4 mm. The spatial resolution of EPI can be higher, with isotropic 2 mm or even 1 mm voxels obtained without shrinking the field-of-view in a larger TR value, or using parallel imaging methods without a larger TR value. The disadvantage of the latter approach would be the noise amplification, as parallel imaging inevitably trades off SNR for resolution enhancement.

The spectrum of GA in EPI-EEG is closely related to the prescribed imaging parameters. It is possible to adjust EPI parameters, including field-of-view, spatial resolution, and the number of slices, to shift these interferences on concurrently acquired EEG signals away from specific frequencies. Other approaches such as accelerating the MRI slice acquisition with no slice gap and synchronizing the MRI and EEG systems per MRI slice instead of per MRI volume can be also helpful. However, such adjustments can be tedious, and calibration measurements may have to be taken before prescribing the experimental protocol, even knowing the dominant frequency of GA from the targeted TR value and number of slices. This is because the GA is not restricted to a narrow frequency range (Fig. 1). Thus, even knowing the dominant frequency of GA, it is difficult to evaluate the extent to which the expected brain signals are overwhelmed by GA without any measurements. Sparsely interleaved fast fMRI-EEG is one approach to alleviate this technical challenge.

Different from our approach, other tailored MRI acquisitions have been proposed to reduce GA. These include spike-driven EEG-MRI (Krakow et al., 1999a; Lazeyras et al., 2000; Lemieux et al., 2001; Warach et al., 1996) and stepping stone sampling (Anami et al., 2003; Freyer et al., 2009). Spike-driven fMRI triggers one MRI volumetric scan upon detecting the offset of the targeted EEG activity. This approach was conceived based on the physiology that the peak of the fMRI response occurs approximately 3–5 s after the neural activity. However, the stability of spike-driven EEG-fMRI time series data may be a concern, because the magnetization may not reach a similar steady state in each volume acquisition (Anami et al., 2003; Herrmann, 2001). The stepping stone sampling method takes EEG samples between each incidence of gradient switching to avoid GA (Anami et al., 2003). This method relies on a highly synchronized clock to turn on and off the EEG sampling, but there is the additional concern that eddy currents due to gradient coil switching can last for hundreds of milliseconds, potentially leaving residual EEG signal artifacts. In comparison, the fast fMRI-EEG method, as implemented with SMS-InI, is relatively simple to implement and does not require tailored on-line EEG processing to trigger or to synchronize between EEG and MRI devices.

Sparsely interleaved imaging has also been proposed for delivering high-quality acoustic stimuli during fMRI (Hall et al., 1999). This is because gradient coil switching not only causes artifacts on EEG, but also introduces strong acoustic noise due to the oscillatory Lorentz forces exerted on the gradient coil inside a strong magnet. When MRI is only activated for image acquisition intermittently, the acoustic noise level is expected to be reduced. Thus, we expect that the proposed sparsely interleaved fast fMRI-EEG method can also reduce concerns related to acoustic noise effects in fMRI experiments, when the auditory stimuli are scheduled during time intervals without gradient coil switching.

Finally, sparsely interleaved fast fMRI and EEG can be particularly useful for concurrent EEG-fMRI recordings where the onset of neural activity is beyond the control of the investigator. For example, in the application of delineating epileptic spike generators, detecting the occurrence of each inter-ictal spike (IIS) is the first step and is critical for subsequent analysis (Gotman et al., 2004; Ives et al., 1993; Krakow et al., 1999b; Seeck et al., 1998). Sparsely interleaved fast fMRI-EEG is expected to facilitate more sensitive and accurate annotation of IIS occurrence, through reduction of GA, leading to more reproducible delineation

of IIS generators. Another potential application involves measuring the inter-subject correlated electrophysiological and hemodynamic activity in response to naturalistic and complex stimuli (Dmochowski et al., 2012; Ki et al., 2016). In such experiments, the stimuli are typically presented continuously, and the targeted brain activity evolves over minutes. Thus, sparsely interleaved fast fMRI-EEG can be a powerful tool to better understand the neurovascular coupling in such experiments.

## Data and code availability

All data used in this study are available via a request to the corresponding author after signing a data sharing agreement approved by National Taiwan University and Sunnybrook Research Institute. Open-access computer code used for this study is available at [https://github.com/fahsuanlin/fhlin\\_toolbox/wiki](https://github.com/fahsuanlin/fhlin_toolbox/wiki).

## CRediT authorship contribution statement

**Hsin-Ju Lee:** Data curation, Writing - original draft, Investigation. **Shu-Yu Huang:** Data curation, Investigation. **Wen-Jui Kuo:** Conceptualization, Writing - review & editing. **Simon J. Graham:** Writing - original draft. **Ying-Hua Chu:** Methodology, Software. **Matti Stenroos:** Software. **Fa-Hsuan Lin:** Conceptualization, Methodology, Software, Writing - original draft, Writing - review & editing, Supervision.

## Acknowledgments

This work was partially supported by the Academy of Finland, Finland (No. 298131), Natural Sciences and Engineering Research Council, Canada (RGPIN-2020-05927), Ministry of Science and Technology, Taiwan (106-2314-B-010 -060 -MY3), National Health Research Institutes, Taiwan (NHRI-EX109- 10905NI).

## References

- Allen, P.J., Josephs, O., Turner, R., 2000. A method for removing imaging artifact from continuous EEG recorded during functional MRI. *Neuroimage* 12, 230–239.
- Allen, P.J., Polizzi, G., Krakow, K., Fish, D.R., Lemieux, L., 1998. Identification of EEG events in the MR scanner: the problem of pulse artifact and a method for its subtraction. *Neuroimage* 8, 229–239.
- Anami, K., Mori, T., Tanaka, F., Kawagoe, Y., Okamoto, J., Yarita, M., Ohnishi, T., Yumoto, M., Matsuda, H., Saitoh, O., 2003. Stepping stone sampling for retrieving artifact-free electroencephalogram during functional magnetic resonance imaging. *Neuroimage* 19, 281–295.
- Babiloni, F., Carducci, F., Cincotti, F., Del Gratta, C., Roberti, G., Romani, G., Rossini, P., Babiloni, C., 2000. Integration of high resolution EEG and functional magnetic resonance in the study of human movement-related potentials. *Methods Archive* 39, 179–182.
- Babiloni, F., Carducci, F., Del Gratta, C., Babiloni, C., Roberti, G., Romani, G., Caltagirone, C., Rossini, P., Urbano, A., 1998. Combined high resolution EEG and functional MRI data for modeling of cortical sources of human movement-related potentials. *Engineering in Medicine and Biology Society. In: 1998. Proceedings of the 20th Annual International Conference of the IEEE. IEEE*, pp. 2135–2138.
- Bayram, A., Bayraktaroglu, Z., Karahan, E., Erdogan, B., Bilgic, B., Özker, M., Kasikci, I., Duru, A.D., Ademoglu, A., Öztürk, C., Arıkan, K., Tarhan, N., Demiralp, T., 2011. Simultaneous EEG/fMRI analysis of the resonance phenomena in steady-state visual evoked responses. *Clin. EEG Neurosci.* 42, 98–106.
- Beldzik, E., Domagalik, A., Beres, A., Marek, T., 2019. Linking visual gamma to task-related brain networks—a simultaneous EEG-fMRI study. *Psychophysiology* 56, e13462.
- Berger, H., 1931. Über das Elektrenkephalogramm des Menschen. *Eur. Arch. Psychiatr. Clin. Neurosci.* 94, 16–60.
- Bonmassar, G., Anami, K., Ives, J., Belliveau, J.W., 1999. Visual evoked potential (VEP) measured by simultaneous 64-channel EEG and 3T fMRI. *Neuroreport* 10, 1893–1897.
- Bonmassar, G., Schwartz, D.P., Liu, A.K., Kwong, K.K., Dale, A.M., Belliveau, J.W., 2001. Spatiotemporal brain imaging of visual-evoked activity using interleaved EEG and fMRI recordings. *Neuroimage* 13, 1035–1043.
- Buxton, R.B., Wong, E.C., Frank, L.R., 1998. Dynamics of blood flow and oxygenation changes during brain activation: the balloon model. *Magn. Reson. Med.* 39, 855–864.
- Buzsaki, G., Wang, X.J., 2012. Mechanisms of gamma oscillations. *Annu. Rev. Neurosci.* 35, 203–225.
- Chen, L., TV, A., Xu, J., Moeller, S., Ugrubil, K., Yacoub, E., Feinberg, D.A., 2015a. Evaluation of highly accelerated simultaneous multi-slice EPI for fMRI. *Neuroimage* 104, 452–459.

- Chen, L., Vu, A.T., Xu, J., Moeller, S., Ugurbil, K., Yacoub, E., Feinberg, D.A., 2015b. Evaluation of highly accelerated simultaneous multi-slice EPI for fMRI. *Neuroimage* 104, 452–459.
- Clark, V.P., Fan, S., Hillyard, S.A., 1994. Identification of early visual evoked potential generators by retinotopic and topographic analyses. *Hum. Brain Mapp.* 2, 170–187.
- Courchesne, E., Hillyard, S.A., Galambos, R., 1975. Stimulus novelty, task relevance and the visual evoked potential in man. *Electroencephalogr. Clin. Neurophysiol.* 39, 131–143.
- Dale, A.M., Liu, A.K., Fischl, B.R., Buckner, R.L., Belliveau, J.W., Lewine, J.D., Halgren, E., 2000. Dynamic statistical parametric mapping: combining fMRI and MEG for high-resolution imaging of cortical activity. *Neuron* 26, 55–67.
- Debener, S., Ullsperger, M., Siegel, M., Engel, A.K., 2006. Single-trial EEG-fMRI reveals the dynamics of cognitive function. *Trends Cognit. Sci.* 10, 558–563.
- Di Russo, F., Martínez, A., Sereno, M.I., Pitzalis, S., Hillyard, S.A., 2002. Cortical sources of the early components of the visual evoked potential. *Hum. Brain Mapp.* 15, 95–111.
- Dmochowski, J.P., Sajda, P., Dias, J., Parra, L.C., 2012. Correlated components of ongoing EEG point to emotionally laden attention - a possible marker of engagement? *Front. Hum. Neurosci.* 6, 112.
- Eason, R.G., 1981. Visual evoked potential correlates of early neural filtering during selective attention. *Bull. Psychonomic Soc.* 18, 203–206.
- Fawcett, T., 2006. An introduction to ROC analysis. *Pattern Recogn. Lett.* 27, 861–874.
- Feinberg, D.A., Setsompop, K., 2013. Ultra-fast MRI of the human brain with simultaneous multi-slice imaging. *J. Magn. Reson.* 229, 90–100.
- Freyer, F., Becker, R., Anami, K., Curio, G., Villringer, A., Ritter, P., 2009. Ultrahigh-frequency EEG during fMRI: pushing the limits of imaging-artifact correction. *Neuroimage* 48, 94–108.
- Goldman, R.I., Stern, J.M., Engel Jr., J., Cohen, M.S., 2000. Acquiring simultaneous EEG and functional MRI. *Clin. Neurophysiol.* 111, 1974–1980.
- Goldman, R.I., Stern, J.M., Engel Jr., J., Cohen, M.S., 2002. Simultaneous EEG and fMRI of the alpha rhythm. *Neuroreport* 13, 2487.
- Gotman, J., Benar, C.G., Dubeau, F., 2004. Combining EEG and fMRI in epilepsy: methodological challenges and clinical results. *J. Clin. Neurophysiol.* 21, 229–240.
- Hall, D.A., Haggard, M.P., Akeroyd, M.A., Palmer, A.R., Summerfield, A.Q., Elliott, M.R., Gurney, E.M., Bowtell, R.W., 1999. "Sparse" temporal sampling in auditory fMRI. *Hum. Brain Mapp.* 7, 213–223.
- Hari, R., Salmelin, R., 1997. Human cortical oscillations: a neuromagnetic view through the skull. *Trends Neurosci.* 20, 44–49.
- Herrmann, C.S., 2001. Human EEG responses to 1–100 Hz flicker: resonance phenomena in visual cortex and their potential correlation to cognitive phenomena. *Exp. Brain Res.* 137, 346–353.
- Hsu, Y.C., Chu, Y.H., Tsai, S.Y., Kuo, W.J., Chang, C.Y., Lin, F.H., 2017. Simultaneous multi-slice inverse imaging of the human brain. *Sci. Rep.* 7, 17019.
- Huster, R.J., Debener, S., Eichele, T., Herrmann, C.S., 2012. Methods for simultaneous EEG-fMRI: an introductory review. *J. Neurosci.* 32, 6053–6060.
- Ives, J.R., Warach, S., Schmitt, F., Edelman, R.R., Schomer, D.L., 1993. Monitoring the patient's EEG during echo planar MRI. *Electroencephalogr. Clin. Neurophysiol.* 87, 417–420.
- Jaccard, P., 1901. Étude comparative de la distribution florale dans une portion des Alpes et des Jura. *Bull. Soc. Vaudoise Sci. Nat.* 37, 547–579.
- Ki, J.J., Kelly, S.P., Parra, L.C., 2016. Attention strongly modulates reliability of neural responses to naturalistic narrative stimuli. *J. Neurosci.* 36, 3092–3101.
- Klitorner, A.L., Graham, S.L., Grigg, J.R., Billson, F.A., 1998. Multifocal topographic visual evoked potential: improving objective detection of local visual field defects. *Invest. Ophthalmol. Vis. Sci.* 39, 937–950.
- Krakow, K., Woermann, F., Symms, M., Allen, P., Lemieux, L., Barker, G., Duncan, J., Fish, D., 1999a. EEG-triggered functional MRI of interictal epileptiform activity in patients with partial seizures. *Brain* 122, 1679–1688.
- Krakow, K., Woermann, F.G., Symms, M.R., Allen, P.J., Lemieux, L., Barker, G.J., Duncan, J.S., Fish, D.R., 1999b. EEG-triggered functional MRI of interictal epileptiform activity in patients with partial seizures. *Brain* 122 (Pt 9), 1679–1688.
- Kruggel, F., Herrmann, C.S., Wiggins, C.J., von Cramon, D.Y., 2001. Hemodynamic and electroencephalographic responses to illusory figures: recording of the evoked potentials during functional MRI. *Neuroimage* 14, 1327–1336.
- Kruggel, F., Wiggins, C.J., Herrmann, C.S., von Cramon, D.Y., 2000. Recording of the event-related potentials during functional MRI at 3.0 Tesla field strength. *Magn. Reson. Med.: Off. J. Int. Soc. Magn. Res. Med.* 44, 277–282.
- Laufs, H., Kleinschmidt, A., Beyerle, A., Eger, E., Salek-Haddadi, A., Preibisch, C., Krakow, K., 2003. EEG-correlated fMRI of human alpha activity. *Neuroimage* 19, 1463–1476.
- Lazeyras, F., Blanke, O., Perrig, S., Zimine, I., Golay, X., Delavelle, J., Michel, C.M., De Tribolet, N., Villemure, J.G., Seeck, M., 2000. EEG-triggered functional MRI in patients with pharmacoresistant epilepsy. *J. Magn. Reson. Imag.* 12, 177–185.
- Lemieux, L., Krakow, K., Fish, D.R., 2001. Comparison of spike-triggered functional MRI BOLD activation and EEG dipole model localization. *Neuroimage* 14, 1097–1104.
- Lin, F.H., Belliveau, J.W., Dale, A.M., Hamalainen, M.S., 2006. Distributed current estimates using cortical orientation constraints. *Hum. Brain Mapp.* 27, 1–13.
- Logothetis, N.K., 2008. What we can do and what we cannot do with fMRI. *Nature* 453, 869–878.
- Mandelkow, H., Brandeis, D., Boesiger, P., 2010. Good practices in EEG-fMRI: the utility of retrospective synchronization and PCA for the removal of MRI gradient artefacts. *Neuroimage* 49, 2287–2303.
- Mandelkow, H., Halder, P., Boesiger, P., Brandeis, D., 2006a. Synchronization facilitates removal of MRI artefacts from concurrent EEG recordings and increases usable bandwidth. *Neuroimage* 32, 1120–1126.
- Mandelkow, H., Halder, P., Boesiger, P., Brandeis, D., 2006b. Synchronization facilitates removal of MRI artefacts from concurrent EEG recordings and increases usable bandwidth. *Neuroimage* 32, 1120–1126.
- Maziero, D., Velasco, T.R., Hunt, N., Payne, E., Lemieux, L., Salmon, C.E., Carmichael, D.W., 2016. Towards motion insensitive EEG-fMRI: correcting motion-induced voltages and gradient artefact instability in EEG using an fMRI prospective motion correction (PMC) system. *Neuroimage* 138, 13–27.
- Mikl, M., Marecek, R., Hlustik, P., Pavlicova, M., Drastich, A., Chlebus, P., Brazdil, M., Krupa, P., 2008. Effects of spatial smoothing on fMRI group inferences. *Magn. Reson. Imaging* 26, 490–503.
- Mulert, C., Lemieux, L., 2009. EEG - fMRI: Physiological Basis, Technique, and Applications. Springer, Berlin Heidelberg.
- Mullinger, K.J., Castellone, P., Bowtell, R., 2013. Best current practice for obtaining high quality EEG data during simultaneous fMRI. *J. Vis. Exp.* 76, e50283.
- Mullinger, K.J., Morgan, P.S., Bowtell, R.W., 2008. Improved artifact correction for combined electroencephalography/functional MRI by means of synchronization and use of vectorcardiogram recordings. *J. Magn. Reson. Imag.* 27, 607–616.
- Mullinger, K.J., Yan, W.X., Bowtell, R., 2011. Reducing the gradient artefact in simultaneous EEG-fMRI by adjusting the subject's axial position. *Neuroimage* 54, 1942–1950.
- Niazy, R.K., Beckmann, C.F., Iannetti, G.D., Brady, J.M., Smith, S.M., 2005. Removal of fMRI environment artifacts from EEG data using optimal basis sets. *Neuroimage* 28, 720–737.
- Niedermeyer, E., da Silva, F.H.L., 2005. *Electroencephalography: Basic Principles, Clinical Applications, and Related Fields*. Lippincott Williams & Wilkins.
- Norcia, A.M., Appelbaum, L.G., Ales, J.M., Cottareau, B.R., Rossion, B., 2015. The steady-state visual evoked potential in vision research: a review. *J. Vis.* 15, 4–4.
- Nunez, P.L., 1981. *Electric Fields of the Brain: The Neurophysics of EEG*. Oxford University Press.
- Ordidge, R., Mansfield, P., Coupland, R., 1981. Rapid biomedical imaging by NMR. *Br. J. Radiol.* 54, 850–855.
- Ordidge, R., Mansfield, P., Doyle, M., Coupland, R., 1982. Real time movie images by NMR. *Br. J. Radiol.* 55, 729–733.
- Ou, W., Nummenmaa, A., Ahveninen, J., Belliveau, J.W., Hämäläinen, M.S., Golland, P., 2010. Multimodal functional imaging using fMRI-informed regional EEG/MEG source estimation. *Neuroimage* 52, 97–108.
- Philiastides, M.G., Sajda, P., 2007. EEG-informed fMRI reveals spatiotemporal characteristics of perceptual decision making. *J. Neurosci.* 27, 13082–13091.
- Riera, J.J., Sumiyoshi, A., 2010. Brain oscillations: ideal scenery to understand the neurovascular coupling. *Curr. Opin. Neurol.* 23, 374–381.
- Ritter, P., Freyer, F., Curio, G., Villringer, A., 2008. High-frequency (600 Hz) population spikes in human EEG delineate thalamic and cortical fMRI activation sites. *Neuroimage* 42, 483–490.
- Rosa, M., Daunizeau, J., Friston, K., 2010. EEG-fMRI integration: a critical review of biophysical modeling and data analysis approaches. *J. Integr. Neurosci.* 9, 453–476.
- Scheeringa, R., Fries, P., Petersson, K.M., Oostenveld, R., Grothe, I., Norris, D.G., Hagoort, P., Bastiaansen, M.C., 2011. Neuronal dynamics underlying high- and low-frequency EEG oscillations contribute independently to the human BOLD signal. *Neuron* 69, 572–583.
- Scheeringa, R., Koopmans, P.J., van Mourik, T., Jensen, O., Norris, D.G., 2016. The relationship between oscillatory EEG activity and the laminar-specific BOLD signal. *Proc. Natl. Acad. Sci. U. S. A.* 113, 6761–6766.
- Seeck, M., Lazeyras, F., Michel, C.M., Blanke, O., Gericke, C.A., Ives, J., Delavelle, J., Golay, X., Haenggeli, C.A., de Tribolet, N., Landis, T., 1998. Non-invasive epileptic focus localization using EEG-triggered functional MRI and electromagnetic tomography. *Electroencephalogr. Clin. Neurophysiol.* 106, 508–512.
- Setsompop, K., Gagoski, B.A., Polimeni, J.R., Witzel, T., Wedeen, V.J., Wald, L.L., 2012. Blipped-controlled aliasing in parallel imaging for simultaneous multislice echo planar imaging with reduced g-factor penalty. *Magn. Reson. Med.* 67, 1210–1224.
- Stenroos, M., Mäntynen, V., Nenonen, J., 2007. A Matlab library for solving quasi-static volume conduction problems using the boundary element method. *Comput. Methods Progr. Biomed.* 88, 256–263.
- Stenroos, M., Nummenmaa, A., 2016. Incorporating and compensating cerebrospinal fluid in surface-based forward models of magneto- and electroencephalography. *PLoS One* 11, e0159595.
- Steyrl, D., Müller-Putz, G.R., 2019. Artifacts in EEG of simultaneous EEG-fMRI: pulse artifact remainders in the gradient artifact template are a source of artifact residuals after average artifact subtraction. *J. Neural. Eng.* 16, 016011.
- Toga, A.W., Mazziotta, J.C., 2002. *Brain Mapping: the Methods*. Elsevier Science.
- Uji, M., Wilson, R., Francis, S.T., Mullinger, K.J., Mayhew, S.D., 2018. Exploring the advantages of multiband fMRI with simultaneous EEG to investigate coupling between gamma frequency neural activity and the BOLD response in humans. *Hum. Brain Mapp.* 39, 1673–1687.
- Ullsperger, M., Debener, S., 2010. *Simultaneous EEG and fMRI: Recording, Analysis, and Application*. Oxford University Press.
- Valdes-Sosa, P.A., Sanchez-Bornot, J.M., Sotero, R.C., Iturria-Medina, Y., Aleman-Gomez, Y., Bosch-Bayard, J., Carbonell, F., Ozaki, T., 2009. Model driven EEG/fMRI fusion of brain oscillations. *Hum. Brain Mapp.* 30, 2701–2721.

- Wan, X., Iwata, K., Riera, J., Kitamura, M., Kawashima, R., 2006. Artifact reduction for simultaneous EEG/fMRI recording: adaptive FIR reduction of imaging artifacts. *Clin. Neurophysiol.* 117, 681–692.
- Warach, S., Ives, J., Schlaug, G., Patel, M., Darby, D., Thangaraj, V., Edelman, R., Schomer, D., 1996. EEG-triggered echo-planar functional MRI in epilepsy. *Neurology* 47, 89–93.
- Zhang, S., Han, X., Chen, X., Wang, Y., Gao, S., Gao, X., 2018. A study on dynamic model of steady-state visual evoked potentials. *J. Neural. Eng.* 15, 046010.
- Zhu, K., Dougherty, R.F., Wu, H., Middione, M.J., Takahashi, A.M., Zhang, T., Pauly, J.M., Kerr, A.B., 2016. Hybrid-space SENSE reconstruction for simultaneous multi-slice MRI. *IEEE Trans. Med. Imag.* 35, 1824–1836.